

RESEARCH PAPERS

A new design method for asymmetrical head gradient coils used for superconducting MRI scanner*

TANG Xin**, ZU Donglin and BAO Shanglian

(Institute of Heavy Ion Physics, and Beijing Key Laboratory of Medical Physics and Engineering, School of Physics, Peking University, Beijing 100871, China)

Received January 3, 2004; revised March 23, 2004

Abstract A novel approach of asymmetrical gradient coil design for head imaging in MRI (magnetic resonance imaging) is presented in this paper. The design is based on a modified target field method in which the stream function is introduced to replace Blaine's scheme for the length control. The transverse head coil calculated by this method has a high performance. The coil efficiency is 0.41 mT/m/A and the inductance is 512 μ H. The coil has an inner diameter of 32 cm and a length of 45.8 cm. The size of the ROU (region of uniformity) is 20 cm along the transverse direction and 17 cm along the axial direction and it is close to one end of the coil. The ROU of the coil matches the ROI (region of interest) of human head very well. Compared with previous designs, our design has relatively high performance and the overlap between the ROU and the ROI is larger (the overlap percent is 95%).

Keywords: MRI, head imaging, gradient coil, target field method, stream function.

High-strength, high-slew-rate gradients produced over the human head are desired in modern MRI (magnetic resonance imaging) for many important imaging applications. For instance, a high b-value in diffusion weighted imaging of human brain for identifying stroke requires a high gradient strength^[1], and the high gradient slew rate is important for the brain-specific application of fMRI (functional MRI) in which high spatial resolution is the main goal^[2]. Therefore, it is desired that optimization methods of head coils will achieve these high coil performances.

Additionally, the design of head coil is constrained by the dimensions of both head and neck. For head coil size, a patient's shoulders limit the access of the head into the coil. Consequently, the ROU (region of uniformity) of the coil cannot match the ROI (region of interest) of the head very well.

Head coils with high performance have been designed by various methods in recent years^[3-6]. Among these designs, the asymmetrical coil scheme proposed by Tomas^[7] overcomes the above-mentioned matching problem and has high coil performance. Tomasi's scheme adopts simulated annealing method which in principle allows complete freedom in

the wire pattern, but it is in practice limited by the computational intensity of the method.

Target field method is a powerful algorithm capable of producing any desired field configuration^[8] and giving coils of the minimum inductance to make coils have high slew rate^[9]. The current constraint condition and the closure constraint condition have been introduced in target field method by Blaine to control the coil length^[10]. With this improvement, gradient coils with small length-to-diameter ratio can be designed for head imaging. However, the Blaine's length control scheme is only effective for symmetrical coils, and it cannot restrict all the current density in the expected region for asymmetrical coils.

Recently, we design a new scheme using the stream function as the constraint condition. The simulations in this paper demonstrate the effectiveness of this scheme on length control of asymmetrical coils. We also present an asymmetrical coil design method for head imaging on the basis of target field method. The head coils designed by this method have high performances and a large ROU, and matches the ROI of the head very well.

* Supported by the National Natural Science Foundation of China (Grant Nos. 10275003 and 19675005)

** To whom correspondence should be addressed. E-mail: tangao7@sina.com

1 Theory

1.1 Target field method

The basis of target field method assumes that the current which is confined to the surface of a cylinder produces the gradient field. The current density is defined as $\mathbf{J}(r, \varphi, z)$. For gradient coils used in MRI, we are only concerned with the z -component of the magnetic field $B_z(r, \varphi, z)$. Note that only the azimuthal component of current density $J_\varphi(\varphi, z)$ contributes to $B_z(r, \varphi, z)$. The Fourier transform of the current density along the azimuthal directions is defined as

$$j_\varphi^m(k) = \frac{1}{2\pi} \int_{-\pi}^{\pi} \varphi e^{-im\phi} \int_{-\infty}^{\infty} dx e^{-ikz} J_\varphi(\varphi, z). \quad (1)$$

Turner defined the relationship between $B_z(r, \varphi, z)$ and the azimuthal component of current density by expanding $B_z(r, \varphi, z)$ in cylindrical harmonics^[8]:

$$B_z(r, \varphi, z) = -\frac{\mu_0 a}{2\pi} \sum_{m=-\infty}^{\infty} \int_{-\infty}^{\infty} dk e^{im\varphi} e^{ikz} \cdot |k| j_\varphi^m(k) \times K_m'(|k| a) I_m(|k| r). \quad (2)$$

The desired magnetic field may be specified at a finite set of points in the coil. It can be written as

$$B_z(r_n, \varphi_n, z_n) = B_n, \quad n = 1, 2, \dots, N. \quad (3)$$

These equations are used as field constraint condition to solve $j_\varphi^m(k)$, then the current density obtained via inverse Fourier transform will give the desired gradient coil which will exactly produce the specified field.

1.2 Coil length control scheme

Blaine introduced the current constraint condition and closure constraint condition into the target field method to control coil length^[10]. The current constraint conditions are employed to force the current density to remain contained within the desired region of the coil surface. They are direct constraints on the values of the azimuthal current density over a set of coordinates, i.e. let

$$J_\varphi(\varphi_p, z_p) = \frac{1}{2\pi} \sum_{-\infty}^{+\infty} \int_{-\infty}^{+\infty} dk \cdot \exp(im\phi_p) \exp(i2\pi k z_p) j_\varphi^m(k) = 0; \quad p = 1, 2, \dots, P. \quad (4)$$

The closure constraint condition prevents any current from crossing the boundaries of a special area on the surface of the coil. A simple form of this constraint condition is to require that the integral of $J_\varphi(\varphi, z)$ on the line along any $\varphi = \varphi_q$ in the region $(-z_q, z_q)$ be zero:

$$\Lambda(\varphi_q, z_q) = \int_{-z_q}^{+z_q} J_\varphi(\varphi_q, z) dz = 0. \quad (5)$$

Both current constraint condition and closure constraint condition are applied in Blaine's length control scheme. Figure 1 shows the scheme applied to a symmetrical coil.

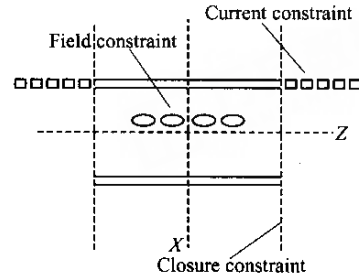


Fig. 1. Schematic diagram of Blaine's length control scheme applied to a symmetrical coil.

In our scheme, the stream function is used as a constraint condition to replace the two conditions mentioned above. Due to the continuity equation $\nabla \cdot \mathbf{J} = 0$, the current density can be expressed as the curl of a vector \mathbf{S} . For current densities flowing on cylindrical surfaces, $\mathbf{J}(\varphi, z)$ can be derived from the radial vector $\mathbf{S} = (S(\varphi, z), 0, 0)$:

$$J_\varphi(\varphi, z) = \frac{\partial}{\partial z} S(\varphi, z),$$

$$J_z(\varphi, z) = -\frac{1}{r} \frac{\partial}{\partial \varphi} S(\varphi, z), \quad (6)$$

where the radial component $S(\varphi, z)$ usually refers to the stream function^[11]. The stream function constraint condition constrains values of the stream function $S(\varphi, z)$ over a set of coordinates outside the bounded region to be zero. From the definition of the stream function, we can see that the use of this constraint provides a sufficient and necessary condition for current density to be zero beyond the bounded region. The stream function of transverse gradient coil can be expressed as $S(\varphi, z) = h(z) \cos \varphi$, then the stream function constraint condition can be written as

$$h(z_p) = 0, \quad p = 1, 2, \dots, P. \quad (7)$$

Figure 2 schematically shows the stream function scheme for length control.

1.3 The asymmetrical coil scheme for head imaging

The gradient uniformity is defined in terms of the percent linearity deviation which is expressed as

$$\alpha = |B_{zc} - B_{zt}| / B_{zt}, \quad (8)$$

where $B_{zc}(r, \varphi, z)$ is the calculated magnetic field distribution and $B_{zt}(r, \varphi, z)$ is the desired magnetic

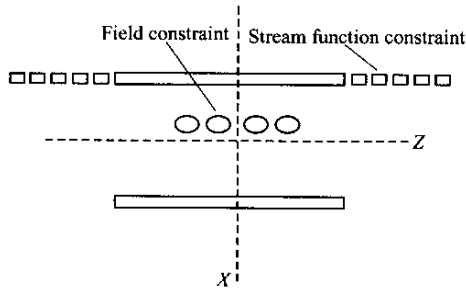


Fig. 2. Schematic diagram of the stream function scheme for length control applied to a symmetrical coil.

field distribution. The α in ROU is usually required to be smaller than 5%. An important parameter of ROU δ is defined as the axial distance between the center of ROU and the edge of the coil. Head coil with the minimum coil diameter is required to increase the gradient efficiency and to reduce the coil inductance. The minimum coil diameter limited by the size of human head and RF coils is larger than 30 cm. The length to diameter ratio of head coils should be larger than 1.5 to achieve enough volume of ROU. The ROU of symmetrical coil is located at the center of the coil, so δ equivalent to the semi-length of the coil is larger than 23 cm. However, the axial average distance between the patients' shoulders and the center of the ROI is shorter than 18 cm. As a consequence, the ROU of symmetrical coils only partially overlaps the ROI. An asymmetrical coil scheme using simulated annealing method was presented by Tomasi recently. ROU is closer to one end of the coil than the other end in the scheme, therefore δ reduces and the overlap region between ROU and ROI increases. The comparison between ROU of symmetrical coil and that of asymmetrical coil is shown in Fig. 3. It can be seen that δ of the asymmetrical coil is smaller than that of symmetrical coil and the matching between ROU and ROI of asymmetrical coil is much better.

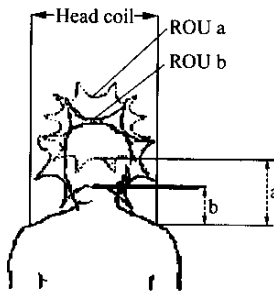


Fig. 3. Comparison between ROU (5% contours of linearity deviation) of symmetrical coil and asymmetrical coil. ROU a is the ROU of the symmetrical head coil; ROU b is the ROU of the asymmetrical coil.

1.4 Asymmetrical head coil design method based on the target field method

The target field method realizes the control of the position of the ROU of coils. The ROU will move closer to one end if the field constraint points move closer to the end, and accordingly an asymmetrical coil design comes into being. The Blaine's length control scheme is not effective for asymmetrical coils. We apply the above-mentioned stream function constraint scheme in this design method. Figure 4 schematically demonstrates our method.

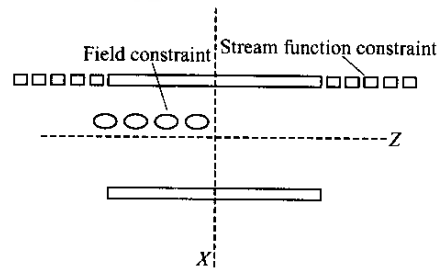


Fig. 4. Schematic diagram of the asymmetrical coil design method.

2 Results and discussions

The Blaine's length control scheme and ours are employed to design an asymmetrical transverse gradient coil, respectively. The coil diameter is 32 cm, and the length to diameter ratio is 1.5. The field constraints are placed at $z_n = [0 \ 2 \ 4 \ 6 \ 8]$ (cm), $r_n = 4$ cm, $\varphi_n = 0$ with $B_n = G_x \cdot r_n$, where G_x is the transverse gradient strength in T/m. For Blaine's scheme, the closure constraint is placed at the desired position z_q and a series of current constraints placed over the adjacent region. Specially, the current constraints are $z_p = \pm [24 + dz \cdot i]$ cm, where $dz = 0.8$ cm; The closure constraint is $z_q = 24$ cm, $\varphi_q = 0$. For our scheme, the set of the stream function constraints are placed at $z_p = \pm [24 + dz \cdot i]$ cm, $i = 0, 1, \dots, 40$. The azimuthal current densities $J_\varphi(z, \varphi = 0)$ are shown in Figs. 5(a) and 5(b), when Blaine's scheme and ours are applied, respectively. These results show that our scheme is effective to force the current density of the asymmetrical coil within the desired region while Blaine's scheme is not.

The discretization of the current distribution in Fig. 5(b) will give the coil loops distribution, and we discrete the current distribution according to Ref. [11]. Figure 6 shows the coil arrangement of the 15 turns in one of the two identical coils on the surface of

the cylindrical former. From this result, the length of the coil can be precisely calculated: $l = 0.458$ m.

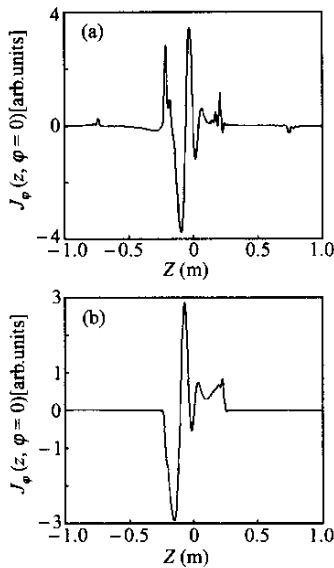


Fig. 5. The azimuthal density distributions of an asymmetrical coil. (a) Distribution applied with Blaine's scheme; (b) distribution applied with the stream function constraint scheme.

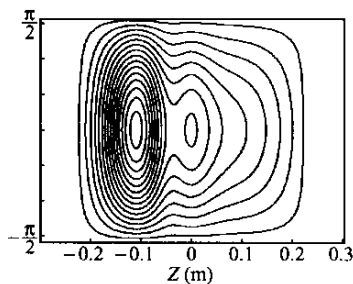


Fig. 6. Asymmetrical transverse gradient coil arrangement.

Fig. 7 is a contour plot which represents the ROU with its percent linearity deviation smaller than

5% in the half coronal plane. The calculation demonstrates that the large ROU with 20 cm along transverse direction and 17 cm along axial direction moves toward one end of the coil. The parameter δ is 15.4 cm for this asymmetrical coil, and the overlap percent between ROU and ROI calculated by assuming a 20 cm ROI along z is 95%.

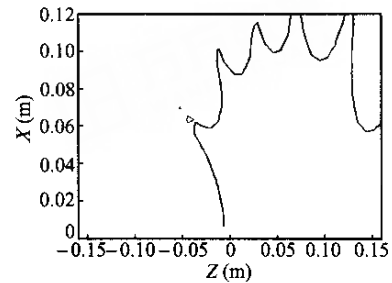


Fig. 7. Contour plot of the 5% ROU produced by the asymmetrical coil in the half coronal plane.

The coil inductance and coil efficiency can be calculated according to Ref.[9]. The coil inductance L is $512 \mu\text{H}$ and the coil efficiency η is 0.41 mT/m/A . The parameter η^2/L is frequently used to quantify the performance of gradient coils because it does not depend on the number of turns in the coils. A larger value of this parameter indicates a higher performance of the coil. The parameter is $3.28 \cdot 10^4 \text{ [T}^2\text{m}^{-2}\text{A}^{-2} \text{H}^{-1} \text{]}$ for this coil. Table 1 compares main parameters of this coil with those of previous asymmetrical coils design for head imaging. The fact that the coil diameter and ROU sizes of various designs are different should be kept in mind when comparing η^2/L . It is clear from the comparison that the design presented in this work has high performance and evident superiority in increasing ROU-ROI matching.

Table 1. Parameters of transverse asymmetrical head coil designs selected from literature

Design	Radius (cm)	Axial length of 5% ROU (cm)	δ (cm)	ROU-ROI matching	$\eta^2/L \times 10^{-4}$ [$\text{T}^2\text{m}^{-2}\text{A}^{-2}\text{H}^{-1}$]
Abduljalif ^[3]	13.6	~15	16.5	~70%	1.57
Alsop ^[4]	16	~16	18	~70%	4.46
Tomas ^[8]	16.8	16	15	~90%	2.35
This work	16	17	15.4	~95%	3.28

3 Conclusions

In principle, by moving the field constraint points toward one end of the coil, the ROU can be arbitrarily close to the end in our method, but in practice, as the ROU moves to one end, the current density near the other end of the coil will increase ac-

cordingly. The increased current density will decrease the coil efficiency η , thereby the value η^2/L will decrease, which indicates the debate of the coil performance. For example, if the field constraints are chosen as: $z_n = [1 \ 3 \ 5 \ 7 \ 9]$ (cm), $r_n = 4$ cm, $\varphi_n = 0$, and the stream function constraints are the same, the efficiency of the calculated coil will be 0.28 mT/m/

A , and the η^2/L will be $1.43 \cdot 10^4$ [$\text{T}^2\text{m}^{-2}\text{A}^{-2}\text{H}^{-1}$]. Here we increase the ROU-ROI matching at the cost of the coil performance, so a compromise between the two properties of the head coil should be carefully pursued in our method.

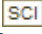
The limitation of human anatomy reduces the overlap between the volume of the coil ROU and the ROI for head imaging. The asymmetrical coil design has been proved to be effective to solve this problem, but previous methods for asymmetrical coil design are limited by the computational intensity of the algorithms. We try to apply the target field method to design asymmetrical head coils here.

The Blaine's scheme for length control used in the target field method is not effective for asymmetrical coils. To replace it, the scheme in which the stream function is introduced as a constraint condition is presented in this work. This scheme manifests itself in length control for asymmetrical coils. Based on this scheme, a new design method for asymmetrical head coil is built up. The coil designed by this method has a high performance and a large volume of ROU which matches the ROI very well. These advantages make our method very suitable for head imaging.

References

- 1 White, M. L. et al. Diffusion imaging utilizing B-values up to 3000 using a high gradient strength scanner in normal subjects and stroke patients. *Radiology*, 1999, 213P : 1477.
- 2 Hennig, J. et al. Functional magnetic resonance imaging : A review of methodological aspects and clinical applications. *Journal of Magnetic Resonance Imaging*, 2003, 18(1): 1.
- 3 Abduljalil, A. M. et al. Torque free asymmetric gradient coils for echo planar imaging. *Magnetic Resonance in Medicine*, 1994, 31 : 450.
- 4 Alsop, D. C. et al. Optimization of torque-balanced asymmetric head gradient coils. *Magnetic Resonance in Medicine*, 1996, 35 : 875.
- 5 Bowtell, R. et al. Analytic approach to the design of transverse gradient coils with co-axial return paths. *Magnetic Resonance in Medicine*, 1999, 41 : 600.
- 6 Blaine, A. et al. Design and fabrication of a three-axis edge ROU head and neck gradient coil. *Magnetic Resonance in Medicine*, 2000, 44 : 955.
- 7 Blaine, A. et al. Constrained length minimum inductance gradient coil design. *Magnetic Resonance in Medicine*, 1998, 39 : 270.
- 8 Tomasi, D. et al. Asymmetrical gradient coil head imaging. *Magnetic Resonance in Medicine*, 2002, 48 : 707.
- 9 Turner, R. A target field approach to optimal coil design. *J. Phys. D : Appl. Phys.*, 1986, L147.
- 10 Turner, R. Minimum inductance coils. *J. Phys. E : Sci. Instrum.*, 1988, 948.
- 11 Turner, R. Gradient coil design : a review of methods. *Magnetic Resonance Imaging*, 1993, 11 : 903.
- 12 Jin, J. M. *Electromagnetic Analysis and Design in Magnetic Resonance Imaging*. Boca Raton : CRC Press LLC, 1998.

A new design method for asymmetrical head gradient coils used for superconducting MRI scanner

作者: [Tang Xin](#), [ZU Donglin](#), [Bao Shanglian](#)
作者单位: [Institute of Heavy Ion Physics, and Beijing Key Laboratory of Medical Physics and Engineering, School of Physics, Peking University, Beijing 100871, China](#)
刊名: [自然科学进展\(英文版\)](#) 
英文刊名: [PROGRESS IN NATURAL SCIENCE](#)
年, 卷(期): 2004, 14(9)
引用次数: 0次

参考文献(12条)

1. [White M L Diffusion imaging utilizing B-values up to 3000 using a high gradient strength scanner in normal subjects and stroke patients](#) 1999
2. [Hennig J Functional magnetic resonance imaging: A review of methodological aspects and clinical applications](#) 2003(1)
3. [Abduljalil A M Torque free asymmetric gradient coils for echo planar imaging](#) 1994
4. [Alsop D C Optimization of torque-balanced asymmetric head gradient coils](#) 1996
5. [Bowtell R Analytic approach to the design of transverse gradient coils with co-axial return paths](#) 1999
6. [Blaine A Design and fabrication of a three-axis edge ROU head and neck gradient coil](#) 2000
7. [Blaine A Constrained length minimum inductance gradient coil design](#) 1998
8. [Tomasi D Asymmetrical gradient coil head imaging](#) 2002
9. [Turner R A target field approach to optimal coil design](#) 1986
10. [Turner R Minimum inductance coils](#) 1988
11. [Turner R Gradient coil design: a review of methods](#) 1993
12. [Jin J M Electromagnetic Analysis and Design in Magnetic Resonance Imaging](#) 1998

相似文献(10条)

1. 外文期刊 [Ibrahim. T.S., Kangarlu. A., Chakeress. D.W. Design and performance issues of RF coils utilized in ultra high field MRI: experimental and numerical evaluations](#)

In this paper, two TEM resonators were evaluated experimentally and numerically at 8 tesla (T) (340 MHz for ^1H imaging). The coils were constructed to be 21.2-cm long (standard) and 11-cm long (a proposed less claustrophobic design). The experimental evaluation was done on a single cadaver using an ultra high field, 8 T, whole-body magnet. The numerical modeling was performed using an in-house finite difference time domain package that treats the coil and the load (anatomically detailed human head model) as a single system. The coils were tested with quadrature excitation at different coil alignment positions with respect to human head. For head imaging at 8 T, the overall numerical and experimental results demonstrated that when compared to the longer coil, the shorter coil provides superior signal-to-noise ratio, coil sensitivity, and excite field in the biological regions that lie within both of the coils' structures. A study of the RF (excite/receive fields) homogeneity showed variations in the performance of both coils that are mostly dependant on the region of interest and the position of coil with respect to the head. As such, depending on the application, the shorter coil could be effectively utilized.

2. 外文期刊 [TANG Xin, ZU Donglin, BAG Shanglian A new design method for asymmetrical head gradient coils used for superconducting MRI scanner](#)

A novel approach of asymmetrical gradient coil design for head imaging in MRI (magnetic resonance imaging) is presented in this paper. The design is based on a modified target field method in which the stream function is introduced to replace Blaine's scheme for the length control. The transverse head coil calculated by this method has a high performance. The coil efficiency is 0.41 mT/m/A and the inductance is 512 μH . The coil has an inner diameter of 32 cm and a length of 45.8 cm. The size of the ROU (region of uniformity) is 20 cm along the transverse direction and 17 cm along the axial direction and it is close to one end of the coil. The ROU of the coil matches the ROI (region of interest) of human head very well. Compared with previous designs, our design has relatively high performance and the overlap between the ROU and the ROI is larger (the overlap percent is 95%).

3. 外文会议 [J.M. vna Oort.E.T. Laskaris.P.S. Thompson.B. Dorri.K.G. Herd A cryogen-free 0.5 tesla mri magnet for head imaging](#)

A compact, cryogen-free 0.5 T superconducting Magnetic Resonance Imager (MRI) magnet for heads and limbs has been developed using conductively-cooled NbTi coils in conjunction with a 4.2 K Gifford-McMahon (GM) refrigerator.

4. 外文期刊 [Goldsmith.IL.Zupanc.ML.Buchhalter.JR Long-term seizure outcome in 74 patients with Lennox-Gastaut syndrome: effects of incorporating MRI head imaging in defining the cryptogenic subgroup.](#)

PURPOSE: To determine if using more stringent criteria for cryptogenic Lennox-Gastaut syndrome (LGS) would result in an improved prognosis for that group. Cryptogenic, symptomatic, and non-cryptogenic LGS patients without etiology (indeterminate) were compared with respect to seizure and cognitive outcome. **METHODS:** Retrospective chart review was performed on 245 patients seen at the Mayo Clinic Rochester from 1976 to 1997, with a diagnosis of either LGS or slow spike wave on EEG. LGS was confirmed in 107 (64 male, 43 female) patients. This group was divided into cryptogenic, symptomatic, and indeterminate groups containing 23, 47, and 37 patients, respectively. In this study, cryptogenic patients all had normal development before onset of LGS, absence of dysmorphic features, normal neurologic examination, and normal magnetic resonance (MRI) brain imaging. Of the 107 patients, 74 had ≥ 3 years of follow-up. **RESULTS:** LGS onset in the 107 patients occurred at a median age of 4.0 years (range, 0.6-28.9 years). When last seen, 63% of those with symptomatic LGS had more than three seizures a day compared with 50% of cryptogenic and 34% of indeterminate patients. The most common seizure types were tonic (77%), atypical absence (61%), and generalized tonic-clonic (56%). Only three patients, all part of the indeterminate group, were seizure free at last follow-up. **CONCLUSIONS:** Using stringent criteria in defining the cryptogenic subgroup resulted in no significant difference in seizure outcome. Individuals with a normal cognitive outcome did not segregate into one etiologic subgroup, but did have LGS onset at an older age.

5. 外文期刊 [Enns GM.Barkovich AJ.Van Kuilenburg AB.Manning M.Sanger T.Witt DR.Van Gennip AH Head imaging abnormalities in dihydropyrimidine dehydrogenase deficiency.](#)

Summary: Dihydropyrimidine dehydrogenase (DPD) deficiency is a rare autosomal recessive disorder of pyrimidine metabolism. Patients may present with a wide range of neurological symptoms during the first years of life. Head imaging abnormalities have been reported only rarely and include diffuse cerebral atrophy and white-matter hyperintensity. The pathogenesis of the white-matter abnormalities is unknown, although environmental factors and altered energy metabolism may be involved. To further understanding of the spectrum of brain abnormalities associated with DPD deficiency, we report a 17-month-old girl, born to a consanguineous Pakistani couple, who had a history of encephalopathy, prolonged hypoventilation, developmental delay and failure to thrive. Head MRI showed prominent sulci and abnormal T2 prolongation in the cerebral white matter and brainstem. Thus, DPD deficiency may feature prominent brain abnormalities involving the cerebral white matter and brainstem. Anoxic stress may have contributed to the clinical presentation and brain findings in this case. In order to define more clearly the contribution of DPD deficiency to the pathogenesis of these MRI abnormalities, we recommend performing detailed analysis of urine pyrimidine metabolites in patients who have such findings.

6. 外文期刊 [Ala TA.Mattson MD.Frey WH 2nd The clinical diagnosis of Alzheimer's disease without the use of head imaging studies. A cliniconeuropathological study.](#)

Although head imaging studies are frequently used in the work-up of dementia, published criteria for the clinical diagnosis of Alzheimer's disease (AD) do not require them. Since our brain bank contains cases in which physicians had specifically diagnosed AD without using a head imaging study, we thought it of interest to investigate the accuracy of their clinical diagnoses. We retrospectively reviewed 911 consecutive dementia cases for those clinically diagnosed as either AD or senile dementia (SD). Twenty-one were identified in which head imaging studies had not been used, each diagnosed as AD or SD by a different physician. In only three had the physician reported a reason why a study was not done. In all 21 cases the primary neuropathological cause of the dementia was AD. Neuropathology in addition to AD was also noted, including cortical Lewy bodies in three, infarcts on gross examination in three, multiple microscopic infarcts in four, and multiple cerebral metastases in one. Acknowledging a number of study limitations, it is remarkable that the judgment of the physicians was correct regarding AD in all 21 cases. It is questionable if a head CT or MRI scan at time of diagnosis would have benefited any of the patients.

7. 外文会议 [Christian Dold.Maxim Zaitsev.Oliver Speck.Evelyn A. Firle.Jurgen Hennig.Georgios Sakas Prospective Head Motion Compensation for MRI by Updating the Gradients and Radio Frequency During Data Acquisition](#)

Subject motion appears to be a limiting factor in numerous magnetic resonance imaging (MRI) applications. For head imaging the subject's ability to maintain the same head position for a considerable period of time places restrictions on the total acquisition time. For healthy individuals this time typically does not exceed 10 minutes and may be considerably reduced in case of pathology. In particular, head tremor, which often accompanies stroke, may render certain high-resolution 2D and 3D techniques inapplicable. Several navigator techniques have been proposed to circumvent the subject motion problem. The most suitable for head imaging appears to be the orbital or spherical navigator methods. Navigators, however, not only lengthen the measurement because of the time required for acquisition of the position information, but also require additional excitation radio frequency (RF) pulses to be incorporated into the sequence timing, which disturbs the steady state. Here we demonstrate the possibility of interfacing the MR scanner with an external optical motion tracking system, capable of determining the object's position with sub-millimeter accuracy and an update rate of 60Hz. The movement information on the object position (head) is used to compensate the motion in real time. This is done by updating the field of view (FOV) by recalculating the gradients and the RF-parameter of the MRI tomograph during the acquisition of k-space data based on the tracking data. Results of rotation phantom, in vivo experiments and the implementation in two different MRI sequences are presented.

8. 外文会议 [Christian Dold.Maxim Zaitsev.Oliver Speck.Evelyn A. Firle.Juergen Hennig.Georgios Sakas. ; Prospective Head Motion Compensation for MRI by Updating the Gradients and Radio Frequency During](#)

Data Acquisition

Subject motion appears to be a limiting factor in numerous magnetic resonance imaging (MRI) applications. For head imaging the subject's ability to maintain the same head position for a considerable period of time places restrictions on the total acquisition time. For healthy individuals this time typically does not exceed 10 minutes and may be considerably reduced in case of pathology. In particular, head tremor, which often accompanies stroke, may render certain high-resolution 2D and 3D techniques inapplicable. Several navigator techniques have been proposed to circumvent the subject motion problem. The most suitable for head imaging appears to be the orbital or spherical navigator methods. Navigators, however, not only lengthen the measurement because of the time required for acquisition of the position information, but also require additional excitation radio frequency (RF) pulses to be incorporated into the sequence timing, which disturbs the steady state. Here we demonstrate the possibility of interfacing the MR scanner with an external optical motion tracking system, capable of determining the object's position with sub-millimeter accuracy and an update rate of 60Hz. The movement information on the object position (head) is used to compensate the motion in real time. This is done by updating the field of view (FOV) by recalculating the gradients and the RF-parameter of the MRI tomograph during the acquisition of k-space data based on the tracking data. Results of rotation phantom, in vivo experiments and the implementation in two different MRI sequences are presented.

9. 外文会议 [Christian Dold](#), [Maxim Zaitsev](#), [Oliver Speck](#), [Evelyn A. Firle](#), [Jürgen Hennig](#), [Georgios Sakas](#)
[Prospective Head Motion Compensation for MRI by Updating the Gradients and Radio Frequency During](#)

Data Acquisition

Subject motion appears to be a limiting factor in numerous magnetic resonance imaging (MRI) applications. For head imaging the subject's ability to maintain the same head position for a considerable period of time places restrictions on the total acquisition time. For healthy individuals this time typically does not exceed 10 minutes and may be considerably reduced in case of pathology. In particular, head tremor, which often accompanies stroke, may render certain high-resolution 2D and 3D techniques inapplicable. Several navigator techniques have been proposed to circumvent the subject motion problem. The most suitable for head imaging appears to be the orbital or spherical navigator methods. Navigators, however, not only lengthen the measurement because of the time required for acquisition of the position information, but also require additional excitation radio frequency (RF) pulses to be incorporated into the sequence timing, which disturbs the steady state. Here we demonstrate the possibility of interfacing the MR scanner with an external optical motion tracking system, capable of determining the object's position with sub-millimeter accuracy and an update rate of 60Hz. The movement information on the object position (head) is used to compensate the motion in real time. This is done by updating the field of view (FOV) by recalculating the gradients and the RF-parameter of the MRI tomograph during the acquisition of k-space data based on the tracking data. Results of rotation phantom, in vivo experiments and the implementation in two different MRI sequences are presented.

10. 外文期刊 [Niemensivu. R.](#), [Pyykko. I.](#), [Valanne. L.](#), [Kentala. E](#) [Value of imaging studies in vertiginous children.](#)

OBJECTIVE: Imaging of the head is expensive and can be stressful for children, some of whom need anesthesia for the procedure. The aim of this study was to determine which vertiginous children benefit most from head imaging. METHODS: We conducted a retrospective chart review of all children aged under 18 years who were referred to the Helsinki University Children's Hospital Radiology Department (tertiary referral center) for head computerized tomography (CT) or magnetic resonance imaging (MRI) over a 1-year period. We analyzed and reviewed the medical records of 87 children who had undergone imaging of the head due to vertigo. RESULTS: Altogether 978 children underwent imaging of the head for various indications. Of these, 87 aged 0-16 years (mean age 8 years) were imaged because of vertigo. Abnormalities were seen in the images of 37 children; 23 were new findings and 14 showed no change in comparison to earlier deviant images. The most common abnormalities in head imaging were brain tumors, infections, multiple sclerosis lesions, and other lesions in T2-weighted images. Of the 23 vertiginous children with a new finding, 19 also had neurological deficits. While four children had no neurological symptoms, three had intense headaches. CONCLUSIONS: Head imaging is necessary for vertiginous children with neurological deficits or persistent headaches or who have sustained a head trauma. If vertigo is the only symptom without trauma, imaging studies will not aid diagnostic work-up.

本文链接: http://d.g.wanfangdata.com.cn/Periodical_zrkJz-e200409002.aspx

下载时间: 2010年3月28日